

Sintering mechanism of Ag nanoparticle-nanoflake a molecular dynamics simulation

Li, Shizhen; Liu, Yang; Ye, Huaiyu; Liu, Xu; Sun, Fenglian; Fan, Xuejun; Zhang, Guoqi

DOI

[10.1016/j.jmrt.2021.12.029](https://doi.org/10.1016/j.jmrt.2021.12.029)

Publication date

2022

Document Version

Final published version

Published in

Journal of Materials Research and Technology

Citation (APA)

Li, S., Liu, Y., Ye, H., Liu, X., Sun, F., Fan, X., & Zhang, G. (2022). Sintering mechanism of Ag nanoparticle-nanoflake: a molecular dynamics simulation. *Journal of Materials Research and Technology*, 16, 640-655. <https://doi.org/10.1016/j.jmrt.2021.12.029>

Important note

To cite this publication, please use the final published version (if applicable).
Please check the document version above.

Copyright

Other than for strictly personal use, it is not permitted to download, forward or distribute the text or part of it, without the consent of the author(s) and/or copyright holder(s), unless the work is under an open content license such as Creative Commons.

Takedown policy

Please contact us and provide details if you believe this document breaches copyrights.
We will remove access to the work immediately and investigate your claim.



Available online at www.sciencedirect.com

jmr&t
Journal of Materials Research and Technology

journal homepage: www.elsevier.com/locate/jmrt



Original Article

Sintering mechanism of Ag nanoparticle-nanoflake: a molecular dynamics simulation



Shizhen Li ^{a,b}, Yang Liu ^{a,*}, Huaiyu Ye ^b, Xu Liu ^c, Fenglian Sun ^a,
Xuejun Fan ^d, Guoqi Zhang ^c

^a School of Material Science and Engineering, Harbin University of Science and Technology, Harbin, China

^b Southern University of Science and Technology, Shenzhen, China

^c Department of Microelectronics, Delft University of Technology, Delft, 2628 CD, the Netherlands

^d Department of Mechanical Engineering, Lamar University, Beaumont, TX, 77710, United States

ARTICLE INFO

Article history:

Received 2 August 2021

Accepted 7 December 2021

Available online 13 December 2021

Keywords:

Molecular dynamics

Nanoparticle

Nanoflake

Sintering

Melting

ABSTRACT

This paper studied the behaviors of sintering between Ag nanoparticle (NP) and nanoflake (NF) in the same size by molecular dynamics simulation. Before the sintering simulation, the melting simulation of NF was carried out to calculate the melting points of NFs and investigate the thermostability of NF. The Lindemann index and potential energy showed that the melting points of NF were significantly size-dependent. During the heating process, the sharp corner of NF transformed to the round corner and could bend spontaneously lower than melting points. In sintering simulation, the sintering process of NF-NP showed a metastable stage before equilibrium. Under low sintering temperature (500 K), the degree of plasticity sintering mechanism of NF-NP was more prominent, which generated more defects, such as amorphous atoms, dislocations, and stacking faults, than NP-NP. The sintered products of NF-NP also presented a better neck size and shrinkage than NP-NP in the same size. A new sintering behavior was observed: NF was bent toward the NP during the sintering. The bending curvature of NF increased as the thickness or the length/width decreased. For the NF with the ratio of length/width to thickness of 5:1, bending could further significantly facilitate neck growth. At 700 K, the plasticity mechanism dominated both the sintering processes of NF-NP and NP-NP. And NF-NP showed a larger diffusivity than NP-NP. At last, we investigated the effects of crystal misorientation, and found that a tilted grain boundary generated in the neck. The NF had the trend of rotation to decrease the crystal misorientation.

© 2021 The Author(s). Published by Elsevier B.V. This is an open access article under the CC BY-NC-ND license (<http://creativecommons.org/licenses/by-nc-nd/4.0/>).

* Corresponding author.

E-mail address: yang_liu@hrbust.edu.cn (Y. Liu).

<https://doi.org/10.1016/j.jmrt.2021.12.029>

2238-7854/© 2021 The Author(s). Published by Elsevier B.V. This is an open access article under the CC BY-NC-ND license (<http://creativecommons.org/licenses/by-nc-nd/4.0/>).

1. Introduction

Nanoparticles (NPs) have lower melting points compared with their counterpart because of their larger surface-to-volume ratio and surface curvature [1,2]. Ag NPs have been widely used in electronics packaging and conductive ink due to their high electrical and thermal conductivity and the property of lower temperature sintering [3–5]. Sintering, as one of the most important methods to form a connection between Ag NPs, many works studied the sintering mechanism of NPs. Cheng et al. [6,7] reported that the plastic deformation mechanism existed in the collision of NPs at room temperature. The collision rate could be controlled by the shapes and sizes of NPs. Wang et al. [8] and Zhang et al. [9] studied the diffusion mechanism of transient liquid phase bonding and monometallic NPs' sintering, respectively. And the influence factors such as the size of NPs, temperature, heating rate, pressure, and crystalline orientation have also been explored during the sintering process [9–13].

The shape of NP as an essential variable has significant effects on sintering behaviors and mechanical properties. Under the low temperature and low-pressure conditions, the sintered Ag nanoflakes (NFs) strength was 30 MPa higher than that of sintered Ag NPs [14]. The shape of NPs can adjust the porosity and pore size of the sintered structure and influence the sintering rate, neck growth mechanism, and diffusivity [15,16]. Mirkoohi et al. [17] simulated the sintering process of sintered pairs composed of sphere NP and other shapes, such as sphere-flake, sphere-nanowire, in molecular dynamics. However, the mechanisms of sintering with different shapes NPs have not been studied. The report shows that the nanocube has the trend that the shape transforms from cube to sphere during the heating process (temperature lower than melting points) [18]. And the NF, as a kind of nanocube with a small thickness, has cubic sharps, which are easy to lose and transform to rounded edges or corners [19]. Therefore, the thermal stability of NF is different from sphere NP. The new sintering mechanisms may be found out during the sintering of NF with NP.

In this simulation, we mainly explored the sintering process between NP and NF based on molecular dynamics. Before the sintering simulation, we conducted a melting simulation to determine the melting points and thermal stabilities of different sizes of NFs, which was helpful for the subsequent sintering simulation design and analysis. In the sintering simulation, the sintering pairs consisting of NF and NP were sintered at 500 K, 600 K, and 700 K to investigate the temperature effect. And we also took into account the crystal misorientation. The shrinkage [20] and the ratio of neck size to the width of NP (x/W) [21] were used to characterize the sinterability of nano pairs. And Mean Square Displacement (MSD) [22] was used to analyze the sintering mechanism and diffusion behaviors.

2. Methods

2.1. Modeling method

In this study, all the simulations were performed in 3 dimensions simulation box with period boundaries. To

investigate the effects of NF's thickness on sintering, Two kinds of length (width)-to-thickness ratios, 5:1 and 5:2, were involved. 5 nm, 7 nm, 9 nm and 11 nm were selected as the length (width) of NFs or the diameters of NPs to study the size effect on the sintering process. Therefore, this study involved 12 kinds of nanostructures. Since pure Ag constructed all the nanostructures, NFs and NPs had the perfect face-centered cubic (FCC) structure at the modeling stage. The configurations of all kinds of NPs and NFs are shown in Table 1. To simplify the description of the behavior of NF, the plane containing the length and thickness and the plane containing the length and width were defined as plane A and plane B.

The P.L. Williams' EAM potential [23] was selected to describe the interaction of atoms. The lattice constant and the melting point measured by this potential were coordinated with the experimental data. The total energy of the system based on this force field is:

$$E_i = F_\alpha \left(\sum_{j \neq i} \rho_\beta(r_{ij}) \right) + \frac{1}{2} \sum_{j \neq i} \varphi_{\alpha\beta}(r_{ij}) \quad (1)$$



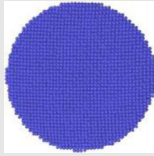
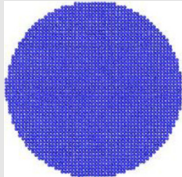

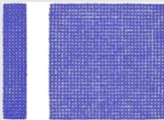
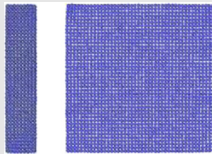
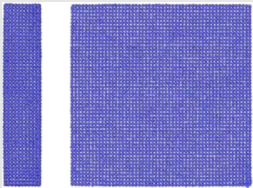
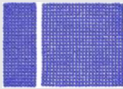
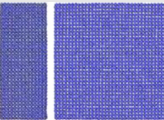
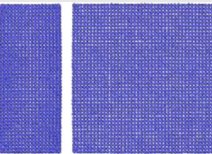
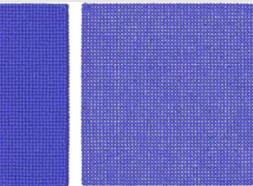
where F is the embedding energy which is a function of ρ , the atomic electron density, φ is a pair potential interaction, α and β are the element types of atoms i and j . Before the melting simulation and the sintering simulation, all the NFs and NPs used the steepest descent algorithm to conduct the energy minimization. After that, the models relaxed at 300 K for 100 ps. According to previous research [24], if the nanostructure became utterly relaxed, it would take hundreds of ns or even several ms. However, the hundreds of relaxation times would cost considerable computing resources. Therefore, we used the metastable NFs and NPs to conduct the simulation. And 1 fs was selected as the timestep.

2.2. Melting and sintering method

Many previous reports [25–27] had studied the thermal stability of the pure Ag NP and their cluster. Therefore, we only conducted the melting simulation of NFs. In melting simulation, the isothermal heating (IH) method [20] was used to eliminate the thermal gradient inside the NF during the heating process. The temperature range was 300 K–1400 K with an interval of 100 K. When the temperature was close to the melting point of NF, the temperature interval was adjusted to 20 K. We found that the nanostructure spent a longer time reaching an equilibrium state at a higher temperature during the melting process. In order to ensure the nanostructures were stable, the NFs were kept at each temperature for 150 ps. The PE evolutions of NFs were shown in S1 (300 K–1400 K, the temperature interval was 100 K) to demonstrate the NFs were equilibrium. We only collected the last 20 ps of data. The NVT ensemble was employed during the melting process, where the temperature was controlled by the Nose–Hoover thermostat.

The chips can be connected with the substrate in the electronic package process by sintering Ag NPs at around 600 K [28]. The higher sintering temperature may damage the chips. Therefore, 500 K, 600 K, and 700 K were selected as the sintering temperature. In sintering simulation, The NFs were the same as the models in melting simulation. Before

Table 1 – The details of 4 types of NPs and 8 types of NFs include the atom numbers and configurations.

Diameter and number of NP	d = 5 nm NP1	d = 7 nm NP2	d = 9 nm NP3	d = 11 nm NP4
Atom number	3819	10,545	22,391	40,902
Configuration				
flake nanoparticle	5*5*1 nm ³ NF1	7*7*1.4 nm ³ NF2	9*9*1.8 nm ³ NF3	11*11*2.2 nm ³ NF4
Atom number	1562	4287	8712	16,038
Configuration				
Size and number of NF	5*5*2 nm ³ NF5	7*7*2.8 nm ³ NF6	9*9*3.6 nm ³ NF7	11*11*4.4 nm ³ NF8
Atom number	3125	8575	17,424	32,076
Configuration				

For each NF, we showed the configurations in two views, where the left figure was the plane A of NF, and the other was the plane B of NF.

sintering, each sintering model was relaxed at the corresponding sintering temperature for 150 ps to reach equilibrium. We combined the NF and NP with the same size (the length/width of NF equal to the diameter of NP) or two equal-size NPs as a nano pair for sintering. The NP faced the center of plane B of NF, as shown in Fig. 1. Before sintering, the gap of NF/NP and NP was 4.085 Å. The sintering time was 500 ps. To eliminate the effects of NF-NP or NP-NP orientation, the NF or NP sintered with NP in <100> orientations [13]. The simulation and the result visualization were performed by LAMMPS [29] and OVITO [30], respectively.

3. Melting simulation

In melting simulation, the melting points of NFs can be determined by potential energy (PE) and Lindemann index (LI) [31]. The LI of atoms in the system is given by

$$\delta_{LI,i} = \frac{1}{N-1} \sum_{j \neq i} \frac{\sqrt{r_{ij}^2 - r_{ij}^2}}{r_{ij}} \quad (2)$$

where N is the total number of atoms in the system, r_{ij} is the distance between atoms i and j , is the ensemble average. The LI of the system is given by

$$\delta_{LI} = \frac{1}{N} \sum_i \delta_{LI,i} \quad (3)$$

The curves of PE per atom and LI of the system evolved with temperature are shown in Fig. 2(a) and (b), respectively. The melting points of NFs can be determined by finding the temperature that the slope of curves has a steep increase in PE and LI temperature. The melting points of eight types of NF are given in Table 2. The melting points determined by both methods roughly agreed with each other. The melting points determined by LI were 20 K higher than that from PE. On the whole, the melting points increased with the volume of NF.

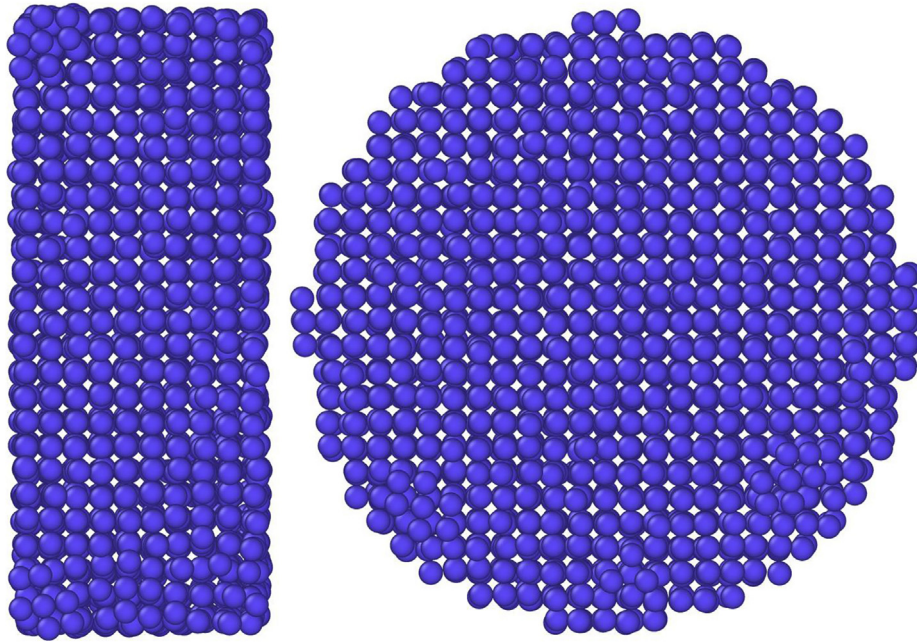


Fig. 1 – The initial configuration of nano pair combined by NF5 and NP1 in sintering simulation.

However, the melting points of NF1, NF2, and NF5 were the same. We suggested that the temperature accuracy near the melting points was 20 K so that we cannot distinguish their melting point from the curves when the melting point difference was less than 20 K. And we also found that the melting points of thinner NF were lower than thicker ones when the NFs had a similar volume. e.g., Although the volumes of NF4 ($N_{\text{atom}} = 16,038$) and NF7 ($N_{\text{atom}} = 17,424$) were similar, the melting point of NF4 was 80 K higher than that of NF4. Similar

results can also be reflected by NF3 and NF6. Therefore, decreasing the thickness of NF can significantly reduce the melting points.

In Fig. 2, we could not only determine the melting points but also analyze the thermal stability of NF. The LI curves fluctuated with different degrees under the melting points. The intensity of the fluctuation varied with the types of NF. And before the beginning of melting, the LI showed a non-linear growth. The NF with a thinner or smaller length/

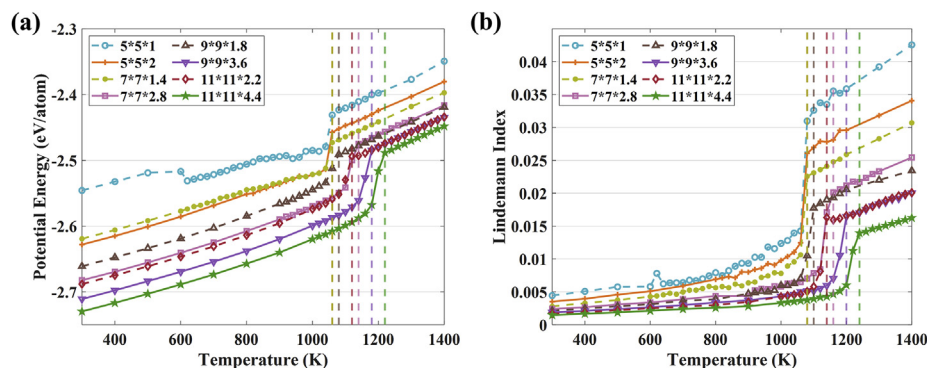


Fig. 2 – (a) The potential energy per atom and (b) the Lindemann Index as functions of temperature for 8 types of NF. The melting point of each NF was presented by the dashed lines with the corresponding color, in which the dashed lines of NF1, NF2, and NF5.

Table 2 – The melting points of eight types NF determined by PE and LI.

NF item	NF1	NF2	NF3	NF4	NF5	NF6	NF7	NF8
Melting points (PE)	1060	1060	1060	1140	1080	1180	1120	1220
Melting points (LI)	1080	1080	1080	1160	1100	1200	1140	1240

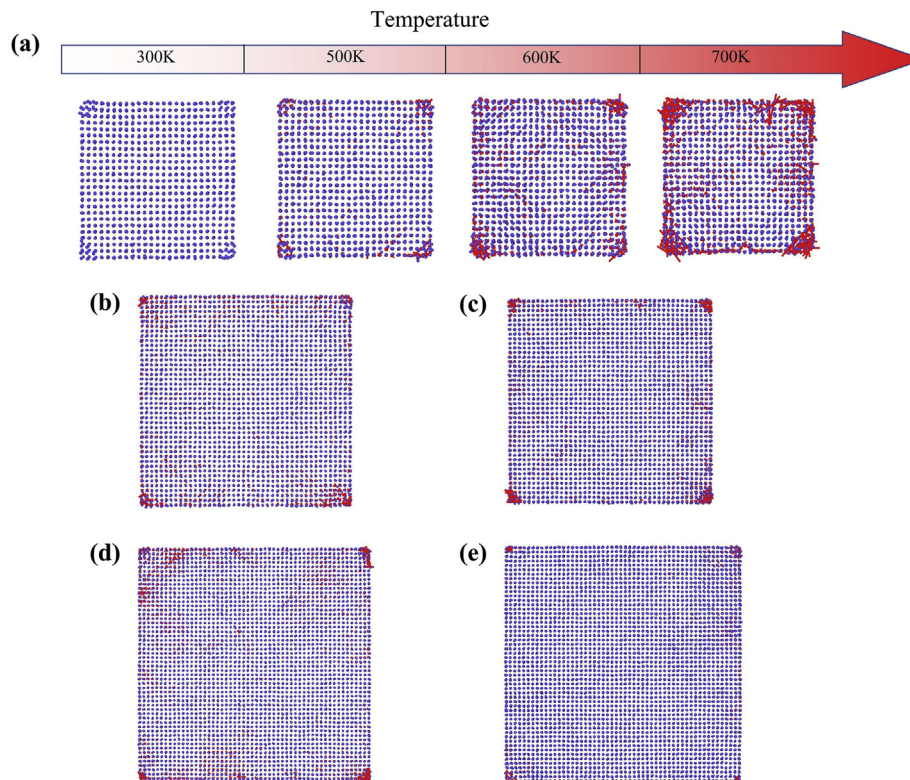


Fig. 3 – (a) The displacement vector of NF5 from 300 K to 700 K. (b)–(e) The displacement vector of (b) NF3, (c) NF7, (d) NF4, (e) NF8 at 500 K based on their configurations of 300 K.

width presented this tendency at a lower temperature because of poorer thermal stability.

To further study the thermal stability and sintering process of NF, we analyzed their behavior during the heating process. The first behavior was that the sharp corner of NF transformed to the round corner at a temperature lower than melting points, which was unique to NF. At a temperature lower than melting points, the sharp corner of NF transformed to the round corner. To illustrate this phenomenon, we showed the displacement vector diagram of NF5 in Fig. 3(a). At first, we got the displacement vector of NF5 at 500 K by taking shape at 300 K as a reference. And then, the displacement vector diagram of the subsequent temperature was generated based on the previous temperature. At 300 K,

the NF5 had sharp corners without transforming to round corners. As the temperature increased to 500 K, the atoms moved, and most of them were concentrated at the four corners. Most atoms located at corners moved along the surface and edge or moved to the inner part of bulk, which leads to the sharp corners transformed to round corners. Except for the corners, a few atoms had displacement behaviors with a small degree on the edge. At 600 K, the area where.

The atoms occurred displacement became larger in the northwest corner. And at 700 K, the range of the atomic displacement continued increasing. The concentrated displacement area transferred to the southeast corner. There were also some atoms located at the north edge also occurred

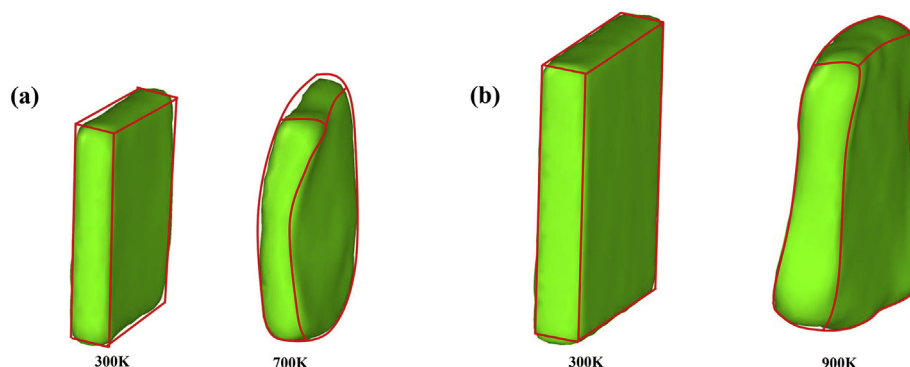


Fig. 4 – The morphology of (a) NF1 and (b) NF2 with construct surface mesh. The red line represented the outline of NFs.

the larger displacement. The decrease of thickness can facilitate the transformation of sharp corners to round corners. This phenomenon can also be observed in large size of NFs such as NF7 and NF8.

Another behavior of NF was that the small size of thin NF could bend spontaneously at higher temperatures. To reflect the evolution of the structure of NF, we used the construct surface mesh to characterize the surface of NF1 and NF2, as shown in Fig. 4. At 300 K, NF1 with a round corner maintained the cube structure. When the temperature increased to 700 K, NF1 exhibited large bending in length and width direction without external force. Even at a lower temperature, such as 500 K, the bulk bending in a small degree had already occurred in NF1. However, it was difficult to observe clearly in picture form. NF2 also had the behavior of bending which degree was smaller than that of NF1.

To further investigate the thermal stability of NFs, we analyzed the LI of atoms of NFs. According to the report [31], if the LI of the atom is larger than the critical value of Lindemann index, the atom was defined as the Lindemann atom (the atom located at melting state). The critical value of the Lindemann index of Ag was 0.07. However, we found that as the temperature reached the melting point, few LIs of atoms were higher than 0.07. Therefore, we redetermined the critical value of LI by selecting the minimum LI of atoms at melting points, as shown in Table 3.

In Fig. 5, we showed the LI of each atom of NFs at 700 K and 1000 K. The NFs with the same size of length/width were placed in a 3-dimension coordinate at 700 K and 1000 K, respectively. In each coordinate system, the upper part was the NF with a ratio of length/width to thickness of 5:1, and the lower part was the NF with a ratio of length/width to thickness of 5:2. The LI of the atom was presented by the corresponding color assigned to the color bar on the right. At 700 K, most atoms' LI of NF larger than 7 nm were maintained low. Some atoms of NF1 and NF5 were characterized as LI atoms since their LI was around the critical value of LI (red spot). This indicated that the premelting occurred.

Because the LI atoms did not appear in other NFs, the premelting process did not occur in NF3 to NF8. We noted that a small number of atoms were characterized as LI atoms on the surface of NF1, NF2, NF3, NF5, and NF6. The premelting occurred in NFs with different degrees. Due to the premelting, the structure of NF1 had lost the regular hexahedron structure, and the area of plane A of NF1 was smaller than that of NF5. At 1000 K (Fig. 5(b)), since the system provided more energy to NF, there were more NF (NF1, NF2, NF3, NF5, NF6)

occurred the surface premelting. And the degree of surface premelting of NF is greater, which induced the trend that the atoms displaced from corner or edge to inner part of NF were more significant than that at 700 K. We could observed that the morphology of NF1 even transformed to a rugby-ball-like.

This melting simulation aimed mainly to assist in designing and analyzing the sintering simulation, and many other facts could influence the thermal stability of NF. Therefore, the exploration of the thermal stability of NF was not our main content. And the task of exhausting all the facts that influence the thermal stability of NF was formidable. The study of the thermal stability of NF could be investigated in future work.

4. Sintering simulation

4.1. The sintering of NF with NP

In the sintering simulation, we used the evolutions of potential energy and the snapshots to analyze the sintering process and shrinkage as well as x/W to define the sintering ability. Shrinkage was defined as the ratio of the changed distance between mass centers of NF and NP to the initial distance, given by:

$$\zeta = \frac{\Delta L}{L_0} = \frac{L_0 - L}{L_0} \quad (4)$$

Where L_0 was the initial distance between the mass centers of NF and NP, L was the distance changing with time. X/W was the ratio of neck size (x) to particle size (W). In this simulation, W was the diameter of NP. Mean square displacement (MSD) was used to determine if the behavior of diffusion occurred, such as surface diffusion or bulk diffusion. The MSD can also verify the existence of the plastic deformation mechanism. MSD can be expressed as follows:

$$\langle d^2 \rangle = \langle \{ [r(t_0 + \gamma) - r_{com}(t_0 + \gamma)] - [r(t_0) - r_{com}(t_0)] \}^2 \rangle \quad (5)$$

Where $\langle \rangle$ is the ensemble average overall time origins, t_0 the time origins, γ the observation time, $r(t_0)$ is the initial atom position, and $r_{com}(t_0)$ is the initial position of CG. This equation has eliminated the effect of CG drift induced by Nosé-Hoover thermostats. Common Neighbor Analyze (CNA) was employed to characterize the local structure evolution. The cutoff distance should be defined before using CNA. The cutoff distance of FCC structure can be expressed as follows:

$$r_{cut}^{fcc} = \frac{1}{2} \left(\sqrt{1/2} + 1 \right) a_{fcc} \approx 0.854 a_{fcc} \quad (6)$$

Where a_{fcc} is the lattice constant of FCC crystal structure, the cutoff radius of Ag was 3.491 Å.

To eliminate the effect of the difference in size between NF and NP, we only simulated the sintering processes of NF5, NF6, NF7, and NF8 sintered with NP which diameter was equal to the length/width of NF. Figure 6(a) (b) was the PE time-dependent evolutions of NF5-NP1 and NP1-NP1. The curves showed that the PE of the sintering of NF-NP decreased more value than that of NP-NP. The PE of NF5-NP1 decreased 0.21eV, while NP1-NP1 only decreased 0.1eV. In the normal sintering process of NPs, the PE time-dependent evolution can be

Table 3 – The critical index of eight types of NFs.

The types of NF	Critical value of LI
NF1	0.0206
NF2	0.0126
NF3	0.0105
NF4	0.094
NF5	0.0155
NF6	0.0104
NF7	0.0082
NF8	0.0068

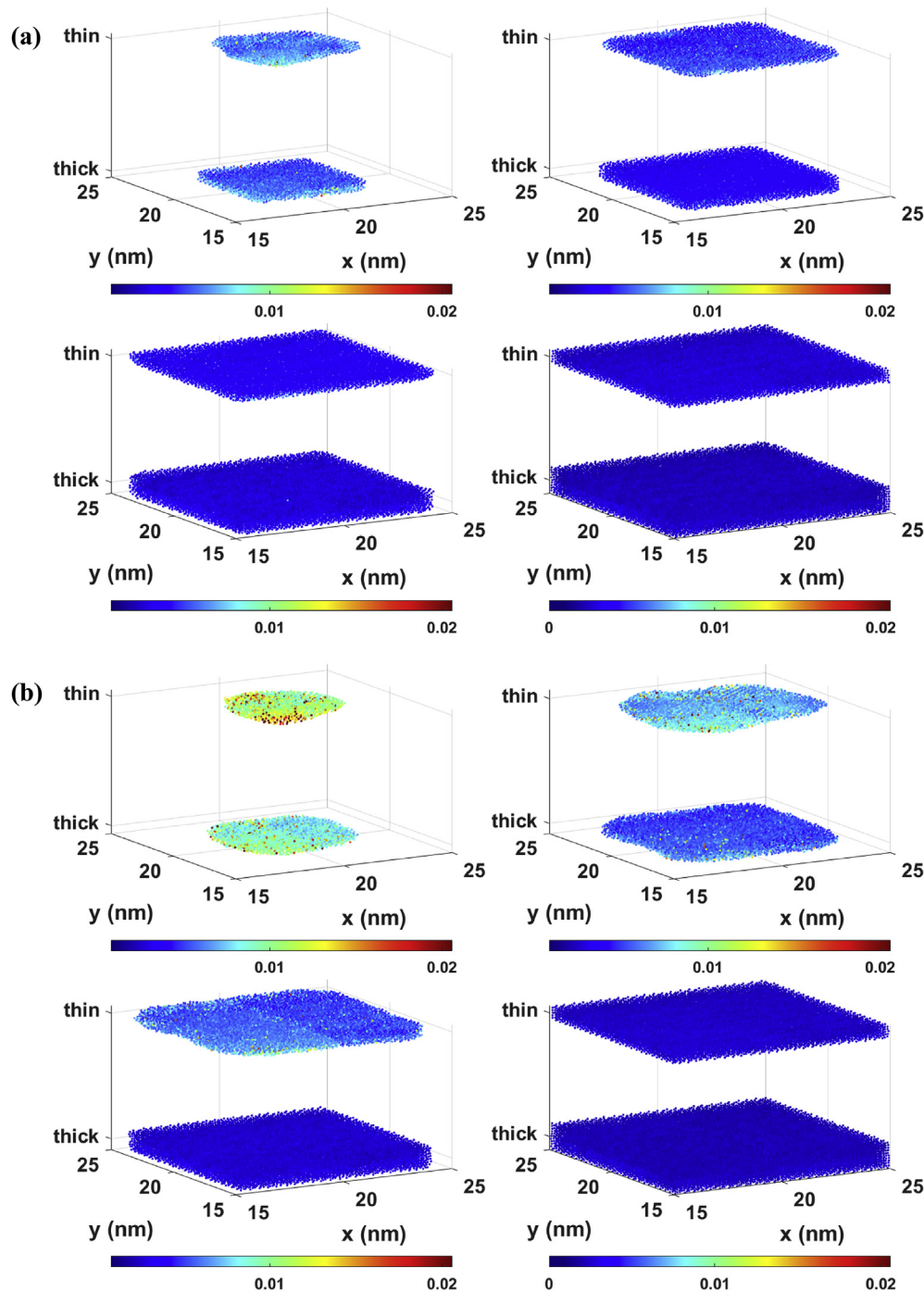


Fig. 5 – The LI of each atom of NFs at (a) 700 K (b) 1000 K. The NF with the same length were placed in the same coordinate system. The upper one is the NF with thin thickness, and the lower one is the NF with thick thickness.

divided into the following three stages: (i) the initial stage is the PE decreased rapidly, (ii) the intermediate stage is the rate of PE evolution became slow, and (iii) the final stage is PE became reached equilibrium. These three stages correspond to shrinkage. The PE time-dependent evolution of NP1-NP1 was very consistent with the above three stages. However, the PE time-dependent evolution of NF5-NP1 can be divided into four stages, as shown in Fig. 6 (a). The initial stage of NF5-NP1 was similar to that of NP1-NP1. Compared with the sintering

process of NP1-NP1, the initial stage of PE evolution of NF5-NP1 lasted for a longer time with a slower rate. The intermediate stage of NF5-NP1 consisted of two sub-stages. In the first sub-stage, PE maintained a metastable state lasting 50 ps. After that, PE entered the second sub-stage and decreased again at about 80 ps. In the end, PE became stable at 99 ps and entered the final stage.

To explore the difference between the sintering processes of NF5-NP1 and NP1-NP1, we analyzed the snapshots of

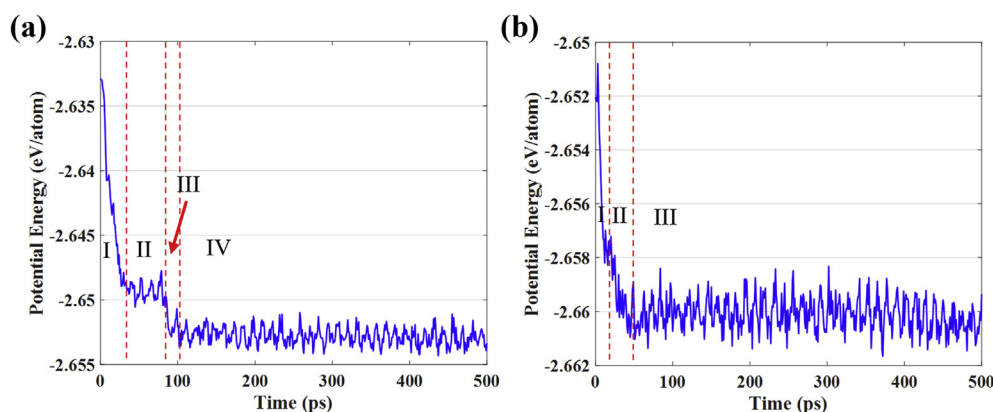


Fig. 6 – The Potential energy evolutions of (a) NF5-NP1 and (b) NP1-NP1. The sintering process of NF5-NP1 and NP1-NP1 can be divided into four and three stages, respectively.

sintering processes of NF5-NP1 (0–99 ps) and NP1-NP1 (0–30 ps), as shown in Fig. 7. The cross-sections of the sintering system the interface mesh of sintered structure combined with dislocation analysis (DXA) were shown in snapshots. In order to simplify the analysis of crystal evolution, we only showed the HCP atoms in the interface mesh. We first analyze the sintering process of NF-NP.

In Fig. 7 (a), before sintering, it was observed that a small number of HCP atoms were scattered in the system because of the small size and metastable structure before sintering (0 ps). At the initial stage, when sintering began, NP and NF contacted each other and formed the neck constructed by amorphous atoms (6 ps). Due to the sintered stress that existed in the neck, two short Shockley dislocations were formed. At 9 ps, the neck grew rapidly. Some atoms transformed from amorphous to FCC structure. The length of dislocation also increased accompanied by generating a few HCP atoms. At 11 ps, the rate of neck growth slowed down. To further decrease the energy induced by the amorphous atoms and optimize the crystallization, the morphology of NF became bending, and the NP rotated clockwise. Under the contribution of sintered stress, there were more dislocations appeared in the neck. Since the sintering temperature of 500 K was not high enough to facilitate the diffusion mechanism, the sintering process was mainly contributed by the plasticity mechanism, i.e., the large stress that existed in the neck region produced various defects. Two stacking faults ((1 -1 1) and (1 1 1)) had formed, which were surrounded by several Shockley dislocations. Since the center of the neck was completed, the A triangular area filled with FCC structure was formed.

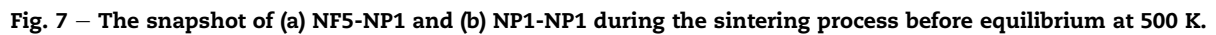
Up to 16 ps, the sintering process entered the first sub-stage of the intermediate stage. The degree of bending of NF reduced. Since the sintered stress still existed in the sintered structure, some new dislocation was generated and a part of Shockley dislocations decomposed into other dislocation that characterized into other dislocation (red). Because the dislocations can cause movement under the contribution of shear stress, Some dislocations moved to the surface or merged with other dislocations. And other dislocations intersected together and formed a junction, which was hard to dissociate (21 ps). The stacking faults were also become larger because of

the interaction of dislocation. At 27 ps, the end of double Shockley dislocation ($1/6 [-2 \ 1 \ -1]$ and $1/6 [-1 \ -1 \ -2]$) at the northeast corner of NP combined into a perfect dislocation. The stacking faults glided and restored FCC structure. At 34 ps, part of perfect dislocation split into two Shockley dislocations again and generated a single stacking fault. At 54 ps, the perfect dislocation completely dissociated. At the second sub-stage of intermediate stage, the stacking fault at the northeast disappeared during the process of the new partial dislocations intersecting together at 84 ps. After that, dislocations in the NP disappeared because of the opposite dislocation vectors (94 ps). Only a single Shockley dislocation left. With the last dislocation moved to the surface, the stacking faults transformed to FCC structure. The sintering process entered the equilibrium stage.

For the sintering structure of NF-NP with a larger size, a similar phenomenon can also be observed. However, due to the larger size of NF and NP had more atoms to participate in the annihilation of defects, The sintering process entered the equilibrium stage in a shorter time. And the details about the behaviors of bending will be analyzed in section 4.2.

For the sintering process of NP1-NP1 (Fig. 7(b)), many past works have reported the sintering process of the double NP model with equal size. Therefore, we only used the sintering of NP5-NP5 as the comparative group. The first different point was that the sintering process of NF-NP spent a longer time than that of NP-NP to reach the equilibrium stage, which had already been illustrated in the previous analysis. The second different point was that there were fewer defects generated during the sintering process. And the interaction of dislocations was fast. Since the temperature or the driven force was not high enough to drive the neck further decreased the curvature of the neck, small stacking faults bounded by a dislocation existed in the upper part of the neck. The transformation of amorphization-crystallization completed rapidly. However, the neck size of NP1-NP1 was smaller than that of NF5-NP1.

To quantify the sintering process, we presented the x/W and the shrinkage of NF-NP and NP-NP from 5 nm to 11 nm as shown in Fig. 8(a) and (b), respectively. The final value of x/W and shrinkage at 500 K, 600 K, and 700 K were listed in Table 4.



NP. We suspected that this result could be attributed to two reasons: (1) the sintering pair consisting of NF and NP had better sintering performance itself. (2) the results of NF-NP calculated by the given equation of shrinkage higher than that of NP-NP if they had the same sintering stability due to the distance in between the center of mass of NF and NP was

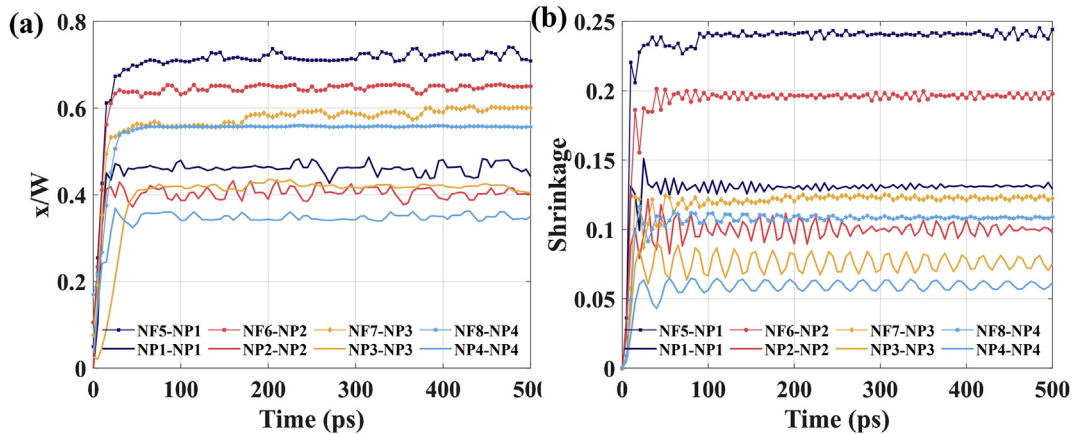


Fig. 8 – The evolutions of (a) x/W and (b) shrinkage for sintering of NF-NP and NP-NP in 4 sizes. The same size of the sintering pairs were presented in the same color. The curves of NF-NP and NP-NP were marked by the line with spot and the line without spot, respectively.

0.3 time smaller than that of NP-NP. According to Table 4, we can conclude that increasing the temperature can generally facilitate the shrinkage and x/W , especially when the temperature rises from 600 K to 700 K and the small size nano pairs. And the sintering process became equilibrium more rapidly under higher temperatures. However, the effect of sintering between nanostructures of different shapes on the final shrinkage and x/W was more significant than that of changing temperature.

In order to investigate the sintering mechanism of NF-NP, we calculated the MSD of NF-NP and NP-NP in four sizes, as shown in Fig. 9 from 500 K to 700 K. The slopes of the curves of MSD were proportional to the diffusion rate. The previous report showed that the rapid increase of MSD in the initial stage contributed to plastic deformation mechanisms. Therefore, we only focus on MSD at the equilibrium stage. At 500 K (Fig. 9(a)), The slopes of MSD curves for all of them were almost 0, which indicated that the self-surface diffusion did not occur. And this result corresponded to other reports. It was also proved indirectly that the plastic deformation mechanism contributed to the sintering process. However, we found that the curve of NF5-NP1 showed a diffusion behavior. We suspected that this diffusion behavior was active by the large curvature in the neck.

At 600 K, a very limited surface diffusion was activated in NF5-NP1, NF6-NP2, and NP1-NP1. However, since the diffusion mechanism was so small that the plastic deformation mechanism still dominated the sintering process, and as the

temperature increased to 700 K, the surface diffusion mechanism can be observed in all the sintering pairs with different diffusivity. Except for the NF6-NP2, the sintering pair of NF-NP showed a larger slope than that of NP-NP in the same size. There are two reasons for the above results. The first reason was that the corner atoms of NF had the trend to move to the bulk of NF, which could facilitate the activity of atoms. The second reason was that the NF showed a more significant thermal stability than NP, as shown in melting simulation.

4.2. The effect of the thickness of NF on sintering of NF-NP

In section 4.1, we only discussed NF in the ratio of length/width to thickness of 5:2. According to the melting simulation results, the NFs with small thickness whereas more active and had lower melting points than that of NF with large thickness if the size of NFs' length/width was the same. And the NF with small size and thickness would bend spontaneously and lose the sharp corner to transform to the round corner by the displacement of atoms under melting point. In this section, we were primarily interested in only discussing the NFs with the ratio of length/width to thickness of difference contributed by the ratio of length/width to thickness 5:2 at 500 K.

Figure 10(a) and 10(b) were the snapshots of the sintering process of NF1-NP1 and NF2-NP2, respectively. Since the structure of NF1 was the most active, the surface of NF1 was not very regular after relaxation. Some atoms in the northwest corner protruded from the surface. Due to the large ratio of

Table 4 – The result of shrinkage and x/W at 500 K, 600 K and 700 K.

Shrinkage	NF5-NP1	NF6-NP2	NF7-NP3	NF8-NP4	NP1-NP1	NP2-NP2	NP3-NP3	NP4-NP4
500 K	0.2	0.15	0.11	0.1	0.115	0.067	0.06	0.05
600 K	0.205	0.153	0.125	0.1	0.13	0.075	0.07	0.055
700 K	0.265	0.195	0.122	0.11	0.13	0.11	0.07	0.058
x/W	NF5-NP1	NF6-NP2	NF7-NP3	NF8-NP4	NP1-NP1	NP2-NP2	NP3-NP3	NP4-NP4
500 K	0.72	0.66	0.59	0.58	0.43	0.4	0.41	0.35
600 K	0.72	0.67	0.59	0.58	0.5	0.4	0.4	0.36
700 K	0.82	0.67	0.64	0.58	0.56	0.45	0.42	0.38

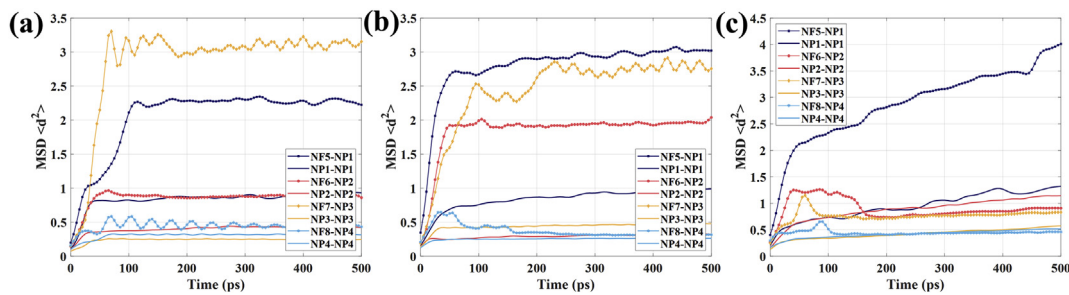


Fig. 9 – The evolutions of MSD of NF-NP and NP-NP in 4 sizes at (a) 500 K, (b) 600 K, (c) 700 K. The color scheme was the same as that in Fig. 8.

surface to the volume, the amorphous atoms had a large proportion, which induced NF1 was more unstable than NF5. Because the thinner NF was easy to deform, NF1 was bent as soon as the NF1 was attached to NP1. And the neck was formed at 4 ps. We can observe that the atoms in the neck region transformed from crystal atoms to amorphous atoms accompanied by the generation of a short dislocation. Although the transformation of NF1-NP1 was similar to that of NF5-NP1, the interaction region of NF1-NP1 was mainly concentrated in NF, which was opposite to NF5-NP1.

At 7 ps, NF1 returned to its original shape. The atoms in the neck further crystal. The dislocations in the neck are moved to the inner of NF. As the sintering progressed, the atoms in both sides of NF1 moved to the neck to facilitate the neck growing (11 ps). However, the degree of bending was so large that the atoms at the upper and lower of the NF connected to the surface of NP and formed a part of the neck. And it was observed that the neck region and the region on the left side of the neck had completely transformed to the FCC structure (11 ps). At 21 ps, the structure became equilibrium. We can find that before the sintering process entered the final stage, with the surface atoms continuing diffusing to the neck, the neck size further increased, which was only 0.5 nm smaller than the diameters of NP. And all the amorphous atoms in the bulk of NF transformed to crystal structure along with a stacking fault.

In the sintering process of NF1-NP1, the effect of bending behavior was more significant. In the case of normal (NF5-NP1), the bending behavior can only change the sintering stress in the neck. However, for NF1-NP1, the bending behavior induced both sides of NF to bend inward with a larger curvature. Therefore, the attachment behavior of both sides of NF seems to be the second sintering, which could provide additional sintering stress to the sintering process.

For the sintering pair of NF2-NP2 (Fig. 10(b)), the ratio of length/width to thickness was the same as NF1. Therefore, we could also observe the same behavior, such as bending toward left then right (5–23 ps), and a part of both sides of NF participated in the sintering process (23–37 ps). And a stacking fault also appeared in the corner of NF. However, since the morphology of NF2 was more stable than that of NF1, the degree of bending behavior was weakened a lot.

Apparently, the bending behavior during the sintering of NF-NP was a necessary process, which could facilitate neck growth. The snapshots of the sintering process of NF-NP

(Fig. 7(a), Fig. 9(a) (b)) indicated that the bending behavior was size-dependent. To detect the size effect on the bending of NF during the sintering process, we calculated the curvature of the surface atoms located on the right side of NF. The steps were as follows:

- (1) Since the position of NF that first contacted with NP was the center of NF on plane B, we selected the middle three-layer as shown in Fig. 11 and got their coordinate data at the beginning of sintering.
- (2) The coordinate data was exported to the two-dimensional coordinate system. To easily fit the atoms coordinate by polynomial model, the x and z coordinate data of atoms location was regarded as y and x coordinate data in the coordinate system used to fit. And we fitted the coordinate to the quadratic polynomial curve.
- (3) According to the quadratic polynomial curve, we calculated the largest curvature of this curve.
- (4) Repeated the steps above and calculated the curvature of the next ps. The atoms distribution with the largest curvature and their fitting curves were shown in Fig. 12(a)
- (5) Selected the maximum value of curvature as the largest curvature of NF during the sintering process and recorded in Fig. 12(b).

Figure 12(b) showed that the maximum curvatures of the NF during the sintering process were highly size-dependent. Firstly, for the diameter of NP (or the length/width of NF) equal to 5, 7, and 11 nm, the curvatures of the thin NFs were almost six times larger than that of thick NFs under the same size. The size of length/width also had an influence on curvature of bending. Especially for the thin NF, the effect of the length/width was not very critical. It was found that the curvature of NF6 was similar to the curvature of NF7. However, for NF1, the bending curvature of NF1 was equal to the surface curvature of NP1. Therefore, the degree of bending was influenced by the size of NF itself and the size of NP. The bending curvature may become larger if NF1 sintered with a smaller NP.

Figure 13 shows the x/W and shrinkage of the nano pairs of NF-NP with 7 nm, 9 nm, 11 nm at 500 K. Due to the NF1 being completely coated on NP1, the neck size and the shrinkage was hard to define and calculate. Therefore, the shrinkage and x/

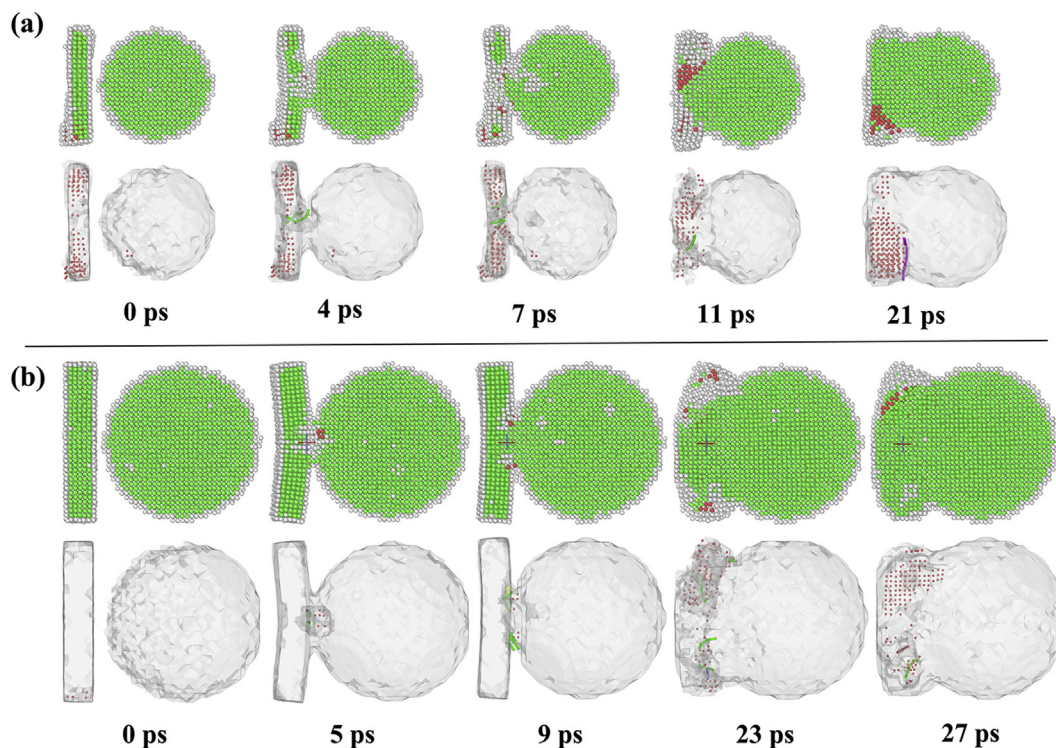


Fig. 10 – The snapshots of (a) NF1-NP1 and (b) NF2-NP2 during the sintering process in initial stage and intermediate stage at 500 K. The color scheme was the same as that of Fig. 7.

W of NF1-NP1 and NF5-NP1 were not presented in Fig. 11. The curves showed that the thickness of NF had a significant effect on the results of x/W and shrinkage. When the diameters of NF are smaller than 11 nm, the decreased thickness can increase more than 30% of the x/W and the shrinkage. However, the effect of thickness on x/W and shrinkage reduced with the increase of the length/width of NF. When the length/width is up to 11 nm, x/W and shrinkage of NF4-NP4 were only 5% larger than these of NF8-NP4.

4.3. The effect of crystal misorientation

In previous sections, we discussed the sintering process of NF-NP without crystal misorientation. However, the crystal

misorientation was common and inevitable in the sintering experiment. Investigating the effect of crystal misorientation was crucial for us to understand the sintering mechanism of NF-NP. Currently, the crystal misorientation with small-angle had already been studied [32]. The large-angle crystal misorientation had not been reported so far. Therefore, in this section, we simulated the sintering process of NF-NP with a large rotation angle. And we mainly studied the effect of crystal misorientation on the sintering process, as shown in Fig. 14.

The initial state of the sintering pair with a 45° misalignment was shown in Fig. 14. At 5ps, the sintering pair was attached to each other. And the neck consisted of amorphous atoms was formed. Since the atom number at initial contact

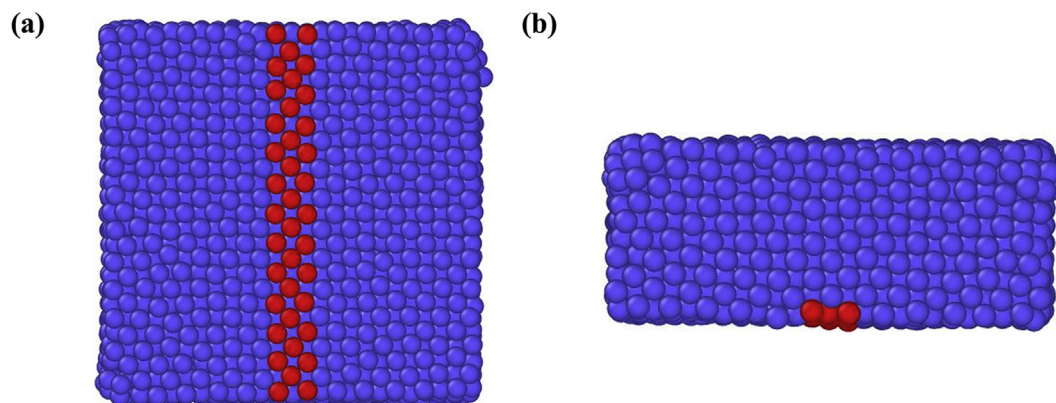


Fig. 11 – The right view (a) and the top view (b) of the surface atoms in the middle three lines that selected to calculate to curvature.

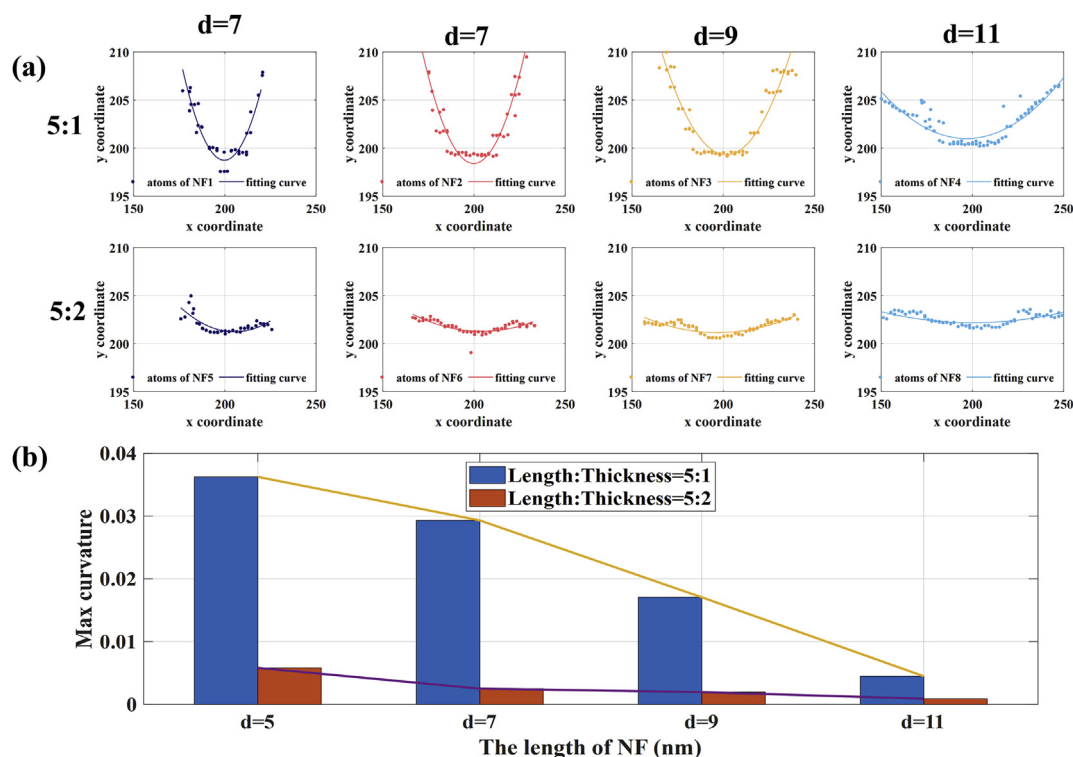


Fig. 12 – (a) The coordinate data of the selected atoms and their fitting results (b) the final curvature calculated from the fitting curves of 8 types of NF.

and arranged orientation of atoms was changed, the degree of amorphous transformation was decreased. The neck grew rapidly. The amorphous-crystallization mechanism did not occur at the initial stage. We observed that the amorphous atoms filled the neck. A tilted grain boundary was formed at the neck because of the rotation of NP. Therefore, the dislocation hardly appeared in the neck. Under the influence of sintered stress and crystal misorientation, the grain boundary was very thick. And we also found a partial dislocation appeared near the neck region, which induced the formation of a small size stacking fault. However, the appearance of dislocation and the stacking faults was short-lived. The

dislocation moved to the grain boundary and the stacking faults transformed to FCC structure, as shown in 16 ps. In order to further decrease the energy of distortion in the neck, some amorphous atoms can also be transformed to FCC without the contribution of dislocation. Therefore, the thickness of the tilted grain boundary was reduced. Since the FCC structure is denser than the amorphous structure, the neck size was also decreased.

From the above behavior and analysis, the driving force of the sintering process of NF-NP with crystal misorientation is divided into two parts, reducing the surface energy and grain boundary energy. However, the large number of amorphous

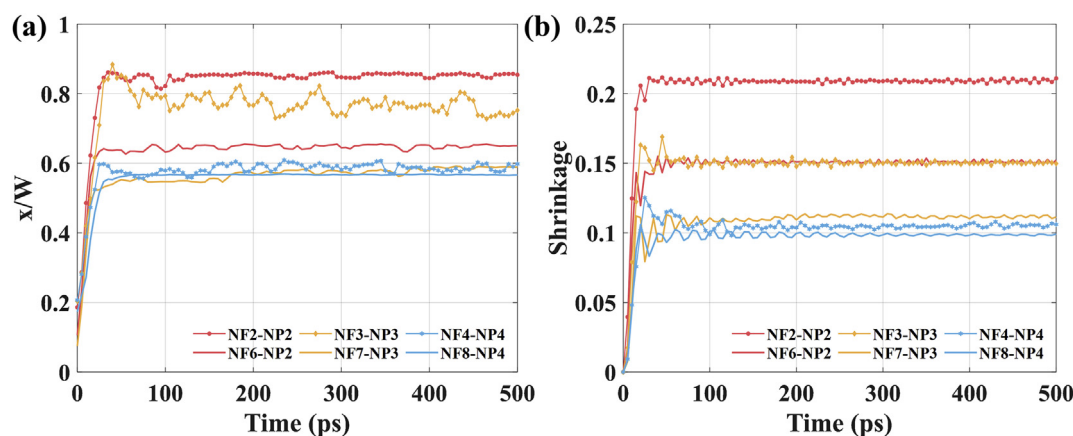


Fig. 13 – The evolution of (a) ratio of neck size to the radius of sphere NP (x/W) and (b) shrinkage for sintering of a sphere with a flack in varying sizes from 7 to 11 nm.

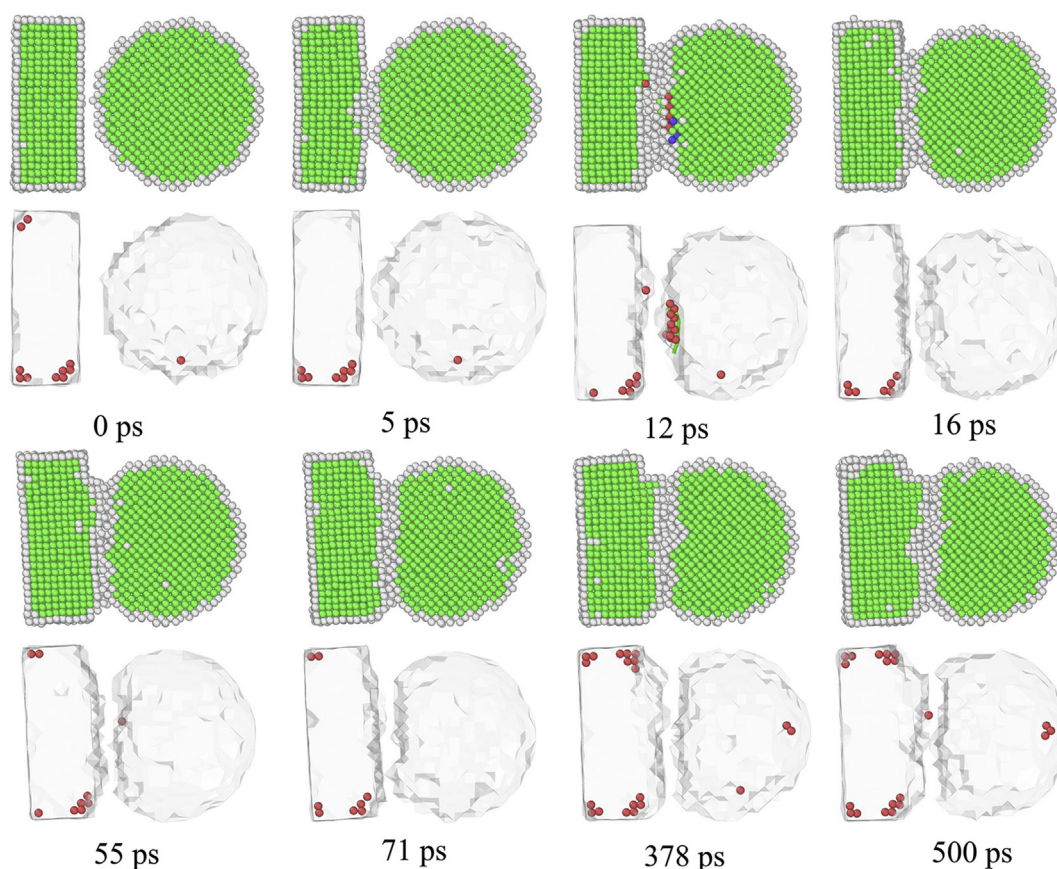


Fig. 14 – The snapshots and interface mesh of NF5-NP1 with 45° crystal misorientation. The color scheme was the same as that of Fig. 7.

atoms transformed to FCC can decrease the neck size and increase the shrinkage. In the following sintering process, we found two interesting behaviors.

The first one was the rotation of NF. After 16 ps, the sintering structure evolution became slow. Due to the crystal misorientation, the NF and NP had the trend of co-alignment [33]. Therefore, at 55 ps, the NP rotated counterclockwise by a small angle to reduce the misorientation. The rotation behavior caused the upside and downside of the neck to suffer

the stretch stress and squeeze stress. A shape that similar to a crack source formed, which led to the curvature of the upside of the neck increased. However, the downside of the neck expanded to continue reducing the surface energy. And at 378 ps, the region contained large curvature that had been filled by surface atoms, which increased the neck size, as shown in Fig. 15(a). We observed that all the curves of NF5–NF8 presented a slow increase. Although the results in 3.2 showed that the surface diffusion had not been activated because of low

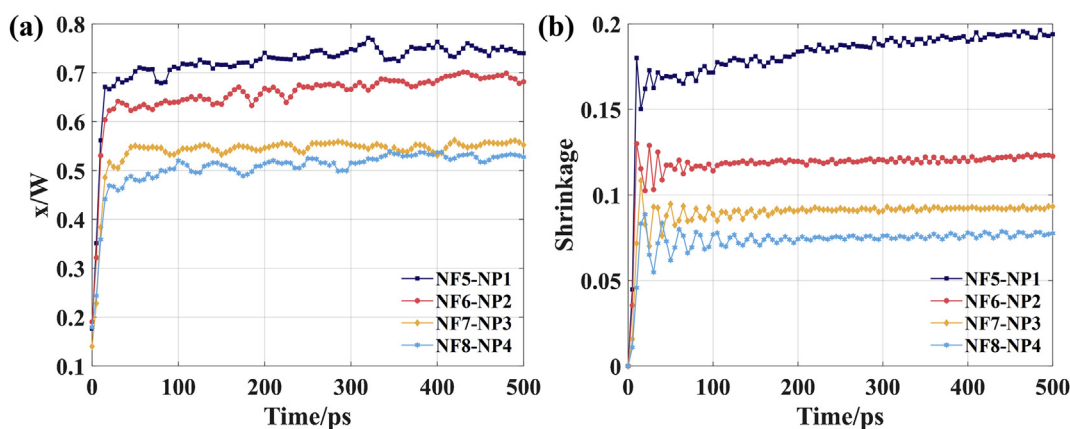


Fig. 15 – (a) The x/W and (b) shrinkage of sintering pairs of NF5-NP1, NF6-NP2, NF7-NP3, NF8-NP4 with 45° crystal misorientation.

temperature, we suggested that the displacement of surface atoms was contributed by the active corner and edge atoms of NF. Although the rotation behavior can also be observed in intermediate stage of sintering of NF5-NP1, the aim of rotation was crystal alignment. NP1 also rotated with NF5. However, in Fig. 14, the crystal orientation of NP1 did not change when NF had already completed the rotation behavior.

The second interesting behavior was the migration of grain boundary. This behavior was also very slow. Before 55 ps, the atoms of NF near the neck had already shown the trend of grain boundary migration. We could observe that the interface between the bulk of NF and the grain boundary was mixed with FCC structure and amorphous structure, which indicated that the migration had not been completed. At 55 ps, the grain boundary migration was first observed and displaced to the direction of NP for 1 atom layer. Until 378 ps, the grain boundary stopped the migration. We suggested that the migration of grain boundary was induced by the rotation of NF.

The evolution of x/W and shrinkage of these four sintering pairs were shown in Fig. 15(a) and (b), respectively. Compared with previous results, when the NF and NP were not aligned with each other, the x/W curves showed a slow fluctuating upward trend after the intermediate stage. However, the crystal misorientation had little effect on the final value of x/W . And for the shrinkage curve, the crystal misorientation had no influence on the evolution process. But as we analyzed before, the existence of grain boundary decreased the densification of the neck, which led to a smaller shrinkage than that of sintered structure with crystal alignment.

In this section, we analyzed the sintering process of NF-NP with crystal misalignment. The process of neck formation and growth, and two unique sintering behaviors, rotation of NF and grain boundary migration, had been reported. However, since the main content of our study was not the effect of crystal misorientation, we did not further analyze it in this section. And the detail and the mechanisms of the effect of crystal misorientation on the sintering process of NF-NP could be continued to investigate in the future.

5. Conclusion

1. In the same ratio of length/width to thickness, the melting point of NF increased with the size. The melting point of NF decreased with thickness for NF with similar volume (atom number). At the temperature far below the melting point, the sharp corner transformed to around the corner. As the temperature close to melting points, the small size of NF with the ratio of length/width to thickness of 5:1 was bent.
2. The sintering process of NF-NP can be divided into four stages: PE decreased rapidly, metastable state, PE decreased at a slow rate, equilibrium. Due to the mismatch of different shapes, more defects were generated during the sintering process. The stacking fault existed in sintered structure can be eliminated by the interaction of dislocations.
3. The x/W and the shrinkage of NF-NP were better than that of NP-NP in the same size. And a new phenomenon that

the NF bent toward NP during the sintering process was found, which was size-dependent. The curvature of NF underwent a bending process increased as the thickness or the length/width decrease. This phenomenon could facilitate the neck size further higher than NF5 and NF6.

4. The crystal misorientation between NF and NP can reduce the x/W and shrinkage due to the tilted grain boundary. Because of missing the dislocation, the dislocation had few effects on the sintering process of NP with crystal misorientation. In order to decrease the crystal distortion induced by misorientation, NF rotated a small angle. This behavior led to more surface atoms diffused to the neck activated by the large curvature generated in the neck.

Declaration of Competing Interest

The authors declare that they have no known competing financial interests or personal relationships that could have appeared to influence the work reported in this paper.

Acknowledgements

This work was supported by the National Natural Science Foundation of China (CN) (51174069), the Shenzhen Fundamental Research Program (JCYJ20200109140822796), and the NSQKJJ under grant K21799119.

Appendix A. Supplementary data

Supplementary data to this article can be found online at <https://doi.org/10.1016/j.jmrt.2021.12.029>.

REFERENCES

- [1] Buffat P, Borel J-P. Size effect on the melting temperature of gold particles. *Phys Rev A* 1976;13:2287–98. <https://doi.org/10.1103/PhysRevA.13.2287>.
- [2] Jiang H, Moon K, Dong H, Hua F, Wong CP. Size-dependent melting properties of tin nanoparticles. *Chem Phys Lett* 2006;429:492–6. <https://doi.org/10.1016/j.cplett.2006.08.027>.
- [3] Corsino DC, Balela MDL. Room temperature sintering of printer silver nanoparticle conductive ink. *IOP Conf Ser Mater Sci Eng* 2017;264. <https://doi.org/10.1088/1757-899X/264/1/012020>.
- [4] Ji H, Zhou J, Liang M, Lu H, Li M. Ultra-low temperature sintering of Cu@Ag core-shell nanoparticle paste by ultrasonic in air for high-temperature power device packaging. *Ultrason Sonochem* 2018;41:375–81. <https://doi.org/10.1016/j.ultsonch.2017.10.003>.
- [5] Dai X, Xu W, Zhang T, Shi H, Wang T. Room temperature sintering of Cu-Ag core-shell nanoparticles conductive inks for printed electronics. *Chem Eng J* 2019;364:310–9. <https://doi.org/10.1016/j.cej.2019.01.186>.
- [6] Cheng B, Ngan AHW. Crystal plasticity of Cu nanocrystals during collision. *Mater Sci Eng* 2013;585:326–34. <https://doi.org/10.1016/j.msea.2013.07.065>.
- [7] Cheng B, Ngan AHW. The sintering and densification behaviour of many copper nanoparticles: a molecular

- dynamics study. *Comput Mater Sci* 2013;74:1–11. <https://doi.org/10.1016/j.commatsci.2013.03.014>.
- [8] Wang J, Shin S, Hu A, Wilt JK. Diffusion kinetics of transient liquid phase bonding of Ni-based superalloy with Ni nanoparticles: a molecular dynamics perspective. *Comput Mater Sci* 2018;152:228–35. <https://doi.org/10.1016/j.commatsci.2018.05.056>.
 - [9] Zhang Y, Zhang J. Sintering phenomena and mechanical strength of nickel based materials in direct metal laser sintering process—a molecular dynamics study, vol. 12; 2016.
 - [10] Yang S, Kim W, Cho M. Molecular dynamics study on the coalescence kinetics and mechanical behavior of nanoporous structure formed by thermal sintering of Cu nanoparticles. *Int J Eng Sci* 2018;123:1–19. <https://doi.org/10.1016/j.ijengsci.2017.11.008>.
 - [11] Yang L, Gan Y, Zhang Y, Chen JK. Molecular dynamics simulation of neck growth in laser sintering of different-sized gold nanoparticles under different heating rates. *Appl Phys A* 2012;106:725–35. <https://doi.org/10.1007/s00339-011-6680-x>.
 - [12] Hu D, Cui Z, Fan J, Fan X, Zhang G. Thermal kinetic and mechanical behaviors of pressure-assisted Cu nanoparticles sintering: a molecular dynamics study. *Results in Physics* 2020;19:103486. <https://doi.org/10.1016/j.rinp.2020.103486>.
 - [13] Nelli D, Rossi G, Wang Z, Palmer RE, Ferrando R. Structure and orientation effects in the coalescence of Au clusters. *Nanoscale* 2020;12:7688–99. <https://doi.org/10.1039/C9NR10163B>.
 - [14] Chen C, Suganuma K. Microstructure and mechanical properties of sintered Ag particles with flake and spherical shape from nano to micro size. *Mater Des* 2019;162:311–21. <https://doi.org/10.1016/j.matdes.2018.11.062>.
 - [15] Miyake K, Hirata Y, Shimonosono T, Sameshima S. The effect of particle shape on sintering behavior and compressive strength of porous alumina. *Materials* 2018;11:1137. <https://doi.org/10.3390/ma11071137>.
 - [16] Nandy J, Sahoo S, Sarangi H. Study on shape dependency of Al-alloy nanoparticles during coalescence in direct metal laser sintering: a molecular dynamics approach. *Mater Today: Proceedings* 2020. <https://doi.org/10.1016/j.matpr.2020.09.557>. S2214785320372734.
 - [17] Mirkoohi E. Effect of shape on nanoparticle sintering: a molecular dynamics study. *Oregon State University*; 2017.
 - [18] Blazhynska MM, Kyrychenko A, Kalugin ON. Molecular dynamics simulation of the size-dependent morphological stability of cubic shape silver nanoparticles. *Mol Simulat* 2018;44:981–91. <https://doi.org/10.1080/08927022.2018.1469751>.
 - [19] Marks LD, Peng L. Nanoparticle shape, thermodynamics and kinetics. *J Phys Condens Matter* 2016;28:053001. <https://doi.org/10.1088/0953-8984/28/5/053001>.
 - [20] Song P, Wen D. Molecular dynamics simulation of the sintering of metallic nanoparticles. *J Nanoparticle Res* 2010;12:823–9. <https://doi.org/10.1007/s11051-009-9718-7>.
 - [21] Kang S-JL. Sintering: densification, grain growth, and microstructure. Amsterdam: Elsevier; 2005.
 - [22] Keffer D, Adhangale P. The composition dependence of self and transport diffusivities from molecular dynamics simulations. *Chem Eng J* 2004;100:51–69. <https://doi.org/10.1016/j.cej.2003.11.028>.
 - [23] Williams PL, Mishin Y, Hamilton JC. An embedded-atom potential for the Cu-Ag system. *Model Simulat Mater Sci Eng* 2006;14:817–33. <https://doi.org/10.1088/0965-0393/14/5/002>.
 - [24] Panizon E, Ferrando R. Strain-induced restructuring of the surface in core@shell nanoalloys. *Nanoscale* 2016;8:15911–9. <https://doi.org/10.1039/C6NR03560D>.
 - [25] Guo JY, Xu CX, Hu AM, Oakes KD, Sheng FY, Shi ZL, et al. Sintering dynamics and thermal stability of novel configurations of Ag clusters. *J Phys Chem Solid* 2012;73:1350–7. <https://doi.org/10.1016/j.jpcs.2012.06.010>.
 - [26] Liang T, Zhou D, Wu Z, Shi P. Size-dependent melting modes and behaviors of Ag nanoparticles: a molecular dynamics study. *Nanotechnology* 2017;28:485704. <https://doi.org/10.1088/1361-6528/aa92ac>.
 - [27] Feng D, Feng Y, Yuan S, Zhang X, Wang G. Melting behavior of Ag nanoparticles and their clusters. *Appl Therm Eng* 2017;111:1457–63. <https://doi.org/10.1016/j.applthermaleng.2016.05.087>.
 - [28] Liu Y, Li Z, Zhang H, Sun F. Microstructure and mechanical properties of nano-Ag sintered joint enhanced by Cu foam. *J Mater Sci Mater Electron* 2019;30:15795–801. <https://doi.org/10.1007/s10854-019-01965-y>.
 - [29] Plimpton S. Fast parallel algorithms for short-range molecular dynamics. *Model Simulat Mater Sci Eng* 2009;18:44. <https://doi.org/10.1006/jcph.1995.1039>.
 - [30] Stukowski A. Visualization and analysis of atomistic simulation data with OVITO—the Open Visualization Tool. *Model Simulat Mater Sci Eng* 2010;18:015012. <https://doi.org/10.1088/0965-0393/18/1/015012>.
 - [31] Tamura Y, Arai N. Molecular dynamics simulation of the melting processes of core–shell and pure nanoparticles. *Mol Simulat* 2015;41:905–12. <https://doi.org/10.1080/08927022.2014.976636>.
 - [32] Zhan L, Zhu X, Qin X, Wu M, Li X. Sintering mechanism of copper nanoparticle sphere-plate of crystal misalignment: a study by molecular dynamics simulations. *J Mater Res Technol* 2021;12:668–78. <https://doi.org/10.1016/j.jmrt.2021.03.029>.
 - [33] Lange AP, Samanta A, Majidi H, Mahajan S, Ging J, Olson TY, et al. Dislocation mediated alignment during metal nanoparticle coalescence. *Acta Mater* 2016;120:364–78. <https://doi.org/10.1016/j.actamat.2016.08.061>.